VALIDATION OF THE REFLECTANCE CALIBRATION OF THE ADS40 AIRBORNE SENSOR USING GROUND REFLECTANCE MEASUREMENTS

U. Beisl [a, *], M. Adiguezel [a]

[a] Leica Geosystems AG, Heerbrugg, Switzerland (Ulrich.Beisl, Muzaffer.Adiguezel)@leica-geosystems.com

Commission VII, WG VII/1

KEY WORDS: Multispectral, Camera, Radiometric, Calibration, Correction, Atmosphere

ABSTRACT:

In the past years digital airborne imaging data have become an appropriate tool to perform remote sensing tasks. With Leica XPro, a processing software for the ADS 40/80 sensor is now available that allows calculating ground reflectance data during rectification. Furthermore, a BRDF correction of the individual flight lines is possible. Since the two processing options are without additional user input, they are also used regularly for mapping purposes to speed up the mosaicking process. In this paper, a validation of the atmospheric correction and reflectance calibration is shown, using data from an image block in southern Germany, which was used in the project "Evaluation of Digital Camera Systems" by the German Society for Photogrammetry, Remote Sensing and Geoinformation (DGPF). Compressed and uncompressed image data was available in 8 and 20 cm ground pixel size together with in-situ ground reflectance measurements of different tarps and natural targets at the time of overflight. Since in the compressed data set the targets were observed several times at different view and illumination angles, also results from the BRDF correction could be compared. The results show a reasonably good agreement between reflectances measured on the ground and those calculated from image data in the atmospheric correction process. Furthermore it could be shown that the BRDF correction option considerably reduces the reflectance difference between different flight lines within selected targets of the test area. The discussion shows the limitations of the method. Finally, improvements are proposed to further increase the accuracy.

1. INTRODUCTION

During the last years there has been a growing interest in the radiometric properties of high-resolution aerial images. An assessment of the radiometric properties of large format digital cameras has been done by Markelin et al. (2008). However, up to now, no operational processes for the handling of absolute radiometric image data are yet implemented in European National Mapping Agencies (Honkavaara et al., 2009).

Attempts to perform an absolute radiometric calibration of frame images have been started for the DMC (Ryan and Pagnutti, 2009, González-Piqueras et al., 2010) and the UltraCam sensors (Alvarez et al., 2010). Molina et al. (2010) are using an empirical polynomial approach to balance the different image brightness in a DMC image mosaic.

The ADS40/80 system features an absolute radiometric calibration since 2006 (Beisl, 2006) and provides a workflow in the Leica XPro software for calculating ground reflectances (Beisl et al., 2008). A validation of the reflectance product is also shown in this symposium (Markelin et al., 2010).

ADS40 data has been used in various remote sensing applications like avalanche prediction (Bühler et al., 2009), classification of benthic habitats (Green and Lopez, 2007), canopy cover and tree species classification (Waser et al., 2008, Waser et al., 2010), urban classification (Emmolo et al., 2008), and archaeological prospection (Kellenberger and Nagy, 2008).

In this article, a validation of the radiometry of the ADS40/80 reflectance and BRDF correction products is done using an image block from a rural area in southern Germany in order to assess the usability of the ADS40/80 system in remote sensing projects. This image block was also used in the project "Evaluation of Digital Camera Systems" by the German Society for Photogrammetry, Remote Sensing and Geoinformation (DGPF). (Cramer, 2010a).

2. MATERIALS AND METHODS

2.1 Leica ADS40/80 sensor

The Leica ADS40/80 sensor uses a line scanner principle, which is particularly suited for absolute radiometric calibration, since the focal plane is temperature stabilized, the lens aperture is fixed, and the CCD lines have a considerably higher dynamic range than any area-CCD. This way a single integration time setting can be used for a whole flight line with heavily varying surface reflectance without the need of changing the aperture.

2.2 Radiometric processing with Leica XPro

Since the dark signal non-uniformity and the photo response non-uniformity (lens falloff) are already corrected on the sensor head, the relation between raw digital numbers (*DN*) and calibrated digital numbers (*CDN*) is just a linear function with a single calibration factor c_1 (camera constant) for each of the 12 CCD lines in a sensor and the actually used integration time (IT [s]). This *CDN* product is the default output of the XPro rectifier ("no correction").

$$CDN = DN * 50 * c_1 / IT \qquad (1)$$

In: Wagner W., Székely, B. (eds.): ISPRS TC VII Symposium – 100 Years ISPRS, Vienna, Austria, July 5–7, 2010, IAPRS, Vol. XXXVIII, Part 7B

Contents   Author Index   Keyword Index

The relation between *CDN* and at-sensor radiances L [W/m^2/sr/µm] is simply

$$L = CDN / 50 \qquad (2)$$

Since at-sensor radiances include all atmospheric effects like the path radiance and the adjacency effect, the images will suffer from a blue hue, which increases towards the borders across the flight direction. Therefore the XPro workflow provides several options for atmospheric correction. The empirical "Dark Pixel Subtraction" and "Modified Chavez Method" will produce approximate ground radiances, which are no surface property because they will still depend on the actual solar illumination.

In order to obtain an image product which is a surface property, in 2008 the "Atmospheric" option has been included in the workflow, which simulates the solar illumination and path radiance, and then calculates reflectance calibrated digital numbers (*RCDN)* (Beisl, 2008). The relation between *RCDN* and reflectance *R* is

$$R = RCDN / 10000 \qquad (3)$$

An additional option is the "BRDF" correction which removes the cross track gradient caused by the reflectance anisotropy of ground surfaces. This correction produces homogeneous image strips calibrated to *RCDN*.

2.3 Airborne data set

In 2008 the DGPF started a project for the "Evaluation of Digital Camera Systems", which included assessments of the geometric and radiometric accuracy performance as well as the performance in generating digital surface models (DSM) and in manual stereo plotting. The project was carried out in the context of the EUROSDR initiative (Cramer, 2010b). A test site at Vaihingen/Enz near Stuttgart (48°56'N, 8°58'E) was chosen and medium format, large format, and hyperspectral cameras were flown by the manufacturers on several days (Cramer, 2010a). The ADS40 S/N 30120 (SH52 type) was flown on August 6, 2010 on two flight altitudes and two configurations (compressed and uncompressed image capture), as given by the DGPF directions (Table 1).

Line	GSD [cm]	Start Time [UTC]	Flight Heading [°]	Sun Azimuth [°]	Sun Zenith [°]	IT RG [ms]	IT BNIR [ms]	Tilt	config
L6	8	0957	90	141.9	37.3	1.448	1.448	N+Bw	comp
L5	8	1002	270	143.7	36.8	1.452	1.452	N+Bw	comp
L4	8	1007	90	145.7	36.3	1.474	1.474	N+Bw	comp
L3	8	1012	270	147.7	35.8	1.476	1.476	N+Bw	comp
L1	8	1028	270	153.8	34.6	1.408	1.408	N+Bw	comp
L7	8	1035	180	156.6	34.1	1.800	1.800	N	raw
L2	8	1039	270	158.6	33.8	1.432	1.432	N+Bw	comp
L8	8	1046	0	161.3	33.4	1.800	1.800	N	raw
H5	20	1054	180	164.9	33.0	4.158	2.908	N	raw
H6	20	1100	0	167.2	32.8	4.482	2.900	N	raw
H4	20	1202	90	195.1	33.0	4.040	2.790	N+Bw	comp
H3	20	1213	90	200.0	33.6	3.866	3.866	N+Bw	comp
H2	20	1228	90	206.1	34.5	3.590	2.340	N+Bw	comp
H1	20	1240	90	210.8	35.5	3.908	2.658	N+Bw	comp

Table 1. Flight lines (L#, H#), solar angles, integration times (IT) for the colour bands, viewing directions (N=nadir, Bw=backward) and compression setting (comp=compressed, raw=uncompressed) for the Vaihingen/Enz data set.

The flight project contained two different data sets: The first data set consisted of E–W flight lines at a lower level (800 m above ground, L#) and a higher level (2000 m, H#), corresponding to a ground sampling distance (GSD) of 8 and 20 cm, respectively. The data was registered in compressed mode and was used for geometric calibration. The second data set with N–S flight lines having 8 and 20 cm GSDs was registered in uncompressed mode, which increased the radiometric resolution, to be most suitable for radiometric validation.

The images, which viewed the radiometric test site (L3, L4, L7, L8, H2, H3, H5, H6) were processed with XPro 4.3 using standard settings to produce three standard products, namely at-sensor radiance (ASR), atmospherically corrected reflectances (ATM), and atmospherically and BRDF corrected reflectances (ATMBRDF).

2.4 Ground measurements

The radiometric calibration accuracy of airborne sensors is difficult to validate with absolute ground radiance measurements since cheap fiber spectrometers tend to drift in the NIR and so a stable absolute calibration for those spectrometers is difficult to obtain. Furthermore, due to changes in atmospheric transmittance the solar irradiance changes rapidly. This means that the measurements have to be taken at the very time of overflight, so measurements at different targets cannot be taken with a single spectrometer. Therefore, reflectance measurements relative to a white calibration standard (e.g. Spectralon®) are performed, instead. This requires modelling the solar irradiance either for calculating the ground radiances from the measured reflectance data or calculating a reflectance product from the image data.

Since the Leica XPro software provides a reflectance product when using the correction with "atmospheric" setting, the validation was done by comparing the XPro image reflectances with measured ground reflectances. This means testing two calibrations of the ADS sensor simultaneously (absolute radiance calibration and reflectance calibration) against the Spectralon calibration and spectrometer stability, i.e. possible deviations cannot be attributed to a single source. However, it makes sense to test the reflectance product that is finally used.

The radiometric test site contained tarps in four colours (white, blue, green, red, provided by RAG Deutsche Steinkohle), 3 Siemens stars for resolution measurements, and a grey wedge tarp, all provided by the University of Stuttgart. The University of Stuttgart made ground measurements with a nadir looking field spectrometer, a camera-based goniometer, and two Sun photometers (Schönermark, 2010).

The day was not optimal for radiometric tests, since high cirrus clouds (altitude > 3 km) passed by frequently. Thanks to an experienced flight crew, the radiometric test site could be imaged without direct cloud shadows except in line H6. However, the aerosol optical thickness (AOT) at 534.3 nm calculated from the Sun photometer data (Figure 1) shows strong haze effects during the time of ground measurements and flights. The AOT was varying between 0.4 and 1 for the different flights resulting in a change of direct solar irradiance by a factor of 1.8. Although this is partially compensated by an increase of the diffuse irradiance, without atmospheric correction, the overall image brightness will vary in this order of magnitude. Since ground reflectance measurements consist of two consecutive measurements of a target and a reference plate, even a small

In: Wagner W., Székely, B. (eds.): ISPRS TC VII Symposium – 100 Years ISPRS, Vienna, Austria, July 5–7, 2010, IAPRS, Vol. XXXVIII, Part 7B

Contents   Author Index   Keyword Index

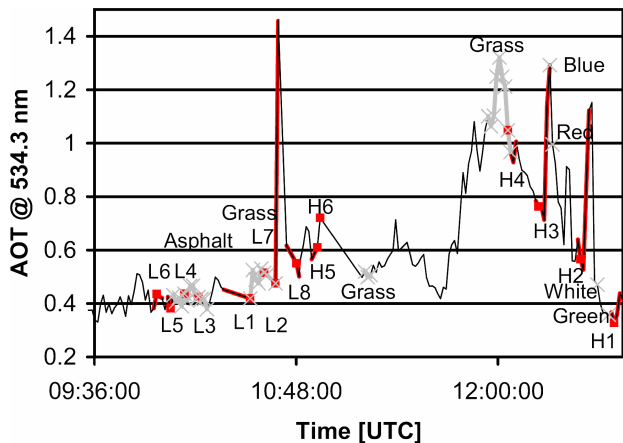irradiance change in between those measurements could cause an error.

Figure 1. Aerosol optical thickness (AOT) at 534.3 nm at the radiometric test site. Red lines with labels L# and H# indicate the AOT values during the whole overflight. The red square indicates the AOT at the time of overpass. The grey lines with crosses depict the AOT during the ground measurements.

The ground reflectance measurements presented in this study were made by the first author on the day of overflight on six targets (Table 2) at the radiometric test site, which was situated at the crossing of the "geometric" E−W and "radiometric" N−S strips (Figure 2). A StellarNet EPP2000 fiber spectrometer with a spectral range of 350−1150 nm and a field of view (FOV) of 8° was used. The measurement distance to the target was 80 cm giving a circle diameter of approximately 11 cm. A 31-cm square Spectralon® plate was used as a reference before each series of target measurements. The solar illuminance was monitored with a luxmeter and whenever it changed by more than 1% a new reference measurement was done.

2.5 Validation method

The relative differences (*RD*) between the reflectances were calculated from the image products ASR, ATM, and ATMBRDF averaged over the ROIs listed in Table 2 and the ground measurements were averaged per target. By theory the atmospheric correction should result in a reduction of the *RD* between ground and image reflectances and between image reflectances of different flight lines:

$$RD = (image - reference)/reference * 100 \quad (4)$$

	Target	# of pixels in H# ROI	Total # of reference measurements	Total # of target measurements	Time [UTC]	Sun Azimuth [°]	Sun Zenith [°]
1	Asphalt_1	3124	4	30	10:14	147.7	35.8
2	Grass_1	28445	9	41	11:17	174.1	32.4
3	White tarp	22	3	6	12:35	208.1	34.9
4	Red tarp	26	1	4	12:23	203.0	34.0
5	Green tarp	23	3	7	12:29	205.5	34.4
6	Blue tarp	26	1	3	12:17	200.7	33.7
7	Asphalt_2	6841					
8	Grass_2	169899					
9	Stubble_1	68215					
10	Stubble_2	186101		No ground measurements			
11	Stubble_3	211972					
12	Stubble_4	47546					
13	Corn	10642					
14	Grass_3	2539					

Table 2. Measured ground reference targets (with measurement time and solar angles) and regions of interest (ROI) in the image data (with number of pixels in the upper altitude H#. The number in the lower altitude L# is higher by a factor of 6.25). The target locations are shown in Figure 2.

3. RESULTS AND DISCUSSION

3.1 Validation of accuracy

The reflectance calibration accuracy was first checked in the spectra of the Asphalt_1 and the Grass_1 target (Figure 3) for all flight lines that contained the target (L3, L4, L7, L8, H2, H3, H5, H8). The agreement is good for the W-E/E-W as well as the N-S/S-N lines in both flying heights. However, there are two exceptions:

First, L4 in nadir view shows a 20% relative increase, and L4 in backward view even a 40% relative increase compared to the ground measurements. The reason is that the nadir sensors view the targets at a scan angle of 20° towards the hot spot, and the backward sensors even at an angle of 25° by geometric addition of the tilt angle. The proximity to the invisible hot spot causes the brightening (In this project, the hot spot cannot be observed in neither flight direction since the maximum ADS scan angle of 32° is always smaller than the Sun zenith angle.).

This brightening is caused by BRDF effects on the ground and is always present in images with changing view angles. For a line scanner like the ADS it can be minimized by selecting targets from the center columns of the image where the view angle is small.

Figure 2. Radiometric test site. Numbers refer to targets and ROIs.

In: Wagner W., Székely, B. (eds.): ISPRS TC VII Symposium – 100 Years ISPRS, Vienna, Austria, July 5–7, 2010, IAPRS, Vol. XXXVIII, Part 7B

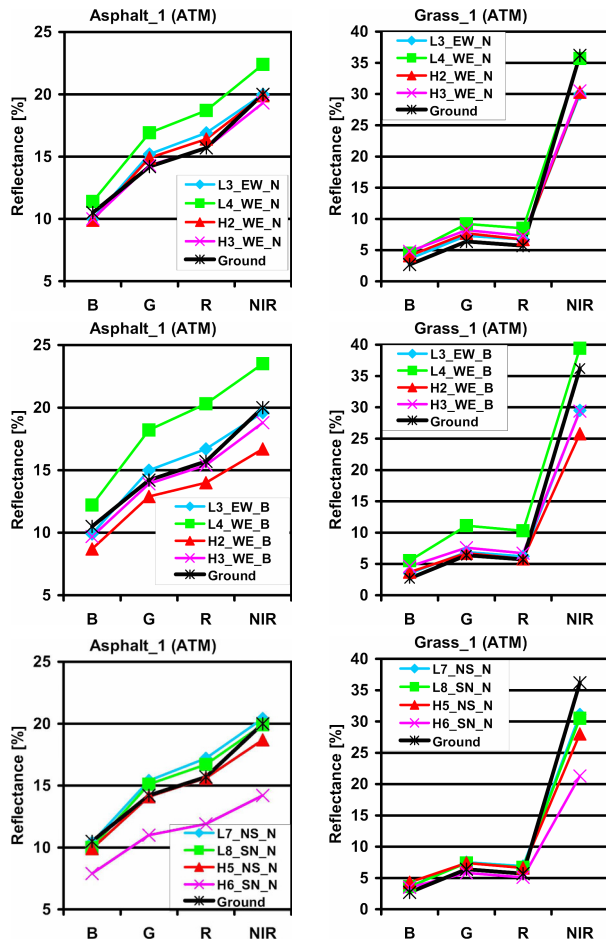Contents   Author Index   Keyword Index

Figure 3. Reflectance spectra calculated from atmospherically corrected images of the Asphalt_1 and Grass_1 target from the nadir (top) and backward (middle) view of the E-W/W-E lines and from the nadir (bottom) view of the N-S/S-N lines compared to ground measurements.

An even better method is to align the flight and sun directions to move the hot spot far away from the observation angles. In our case this would result in selecting the N-S/S-N rather than the E-W/W-E flight lines. Figure 3 shows that flight lines perpendicular to the Sun direction (L3, L4, H2, H3) had strong BRDF effects, while flight lines in the Sun direction (L7, L8, H5, H6) had small BRDF effects, i.e. the reflectances are closer to the ground measurements, which were taken from nadir.

Second, although line H6 was flown in N–S direction and the targets are positioned in the center columns of the image, there is a strong relative discrepancy of 40% especially for the asphalt target. This can be explained by the presence of clouds and an increase of AOT, which can be seen from Figure 1. This causes a decrease in apparent reflectance. To compensate the effects of local AOT variations in the images, simultaneous irradiance measurements on the aircraft would be needed.

For a more quantitative analysis of the accuracy, two flight lines (L7, H5) were selected, since they had no apparent BRDF effects and were both flown in the N–S direction. The *RD* between the averaged image reflectances and the ground measurements depends very much on the type of target used (Figure 4). Target Asphalt_1 shows deviations of below 10%, while Grass_1 and the colour tarps show deviations of up to 50% in both the upper and lower flight lines. A possible cause could be

the small number of pixels that were available for the colour tarp ROIs in the upper level and the small number of target measurements (Table 2). However, the deviations are comparable also for the lower level, so this can be ruled out most likely.
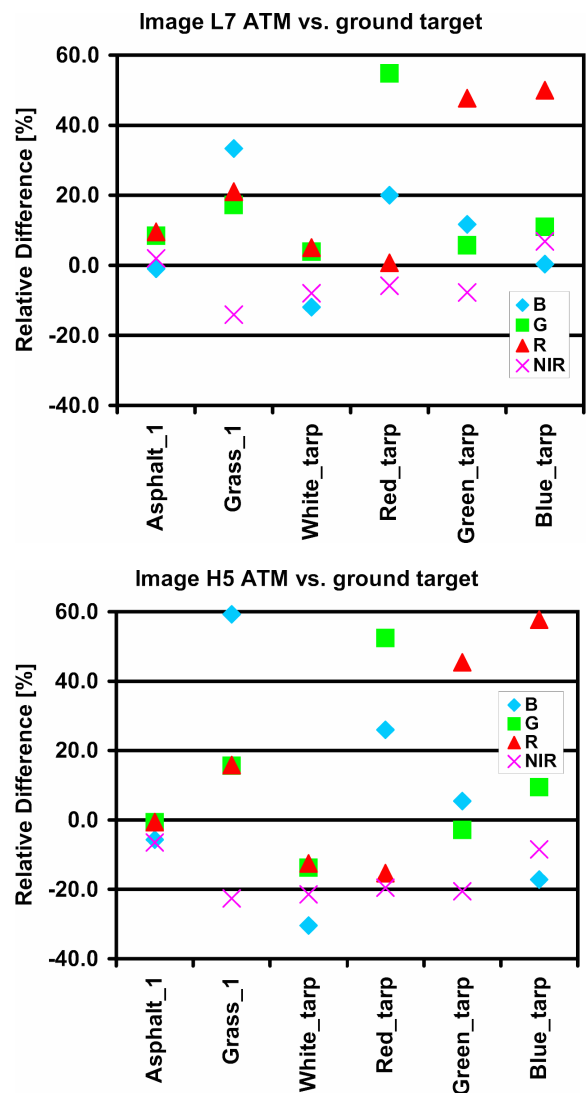

Figure 4. Relative differences of averaged image reflectances and ground reflectance measurements for two flight altitudes L7 (top) and H5 (bottom).

So the effect has to be explained in both cases by combined BRDF and atmospheric effects (Figure 1). For the colour tarps, strong reflectance anisotropy was apparent already by visual inspection (Schönermark, 2010), although they appear uniform when viewed from *one* direction. The view angle is the same for L7, H5, and ground measurements, but the sun position has changed between the overflight and the ground measurements, which also affects BRDF. The main reason for the discrepancies may be the unstable atmospheric conditions at the time of the ground measurements of the tarps. For the Grass_1 target we have to assume strong reflectance anisotropy, also changing with daytime. In addition, due to the current measurement setup (laboratory table with wheels and a 1m boom holding the spectrometer) a good portion of the hemisphere, which would illuminate the object diffusely, was covered by the measurement apparatus. So the diffuse illumination was different for images and ground measurements.

In: Wagner W., Székely, B. (eds.): ISPRS TC VII Symposium – 100 Years ISPRS, Vienna, Austria, July 5–7, 2010, IAPRS, Vol. XXXVIII, Part 7B
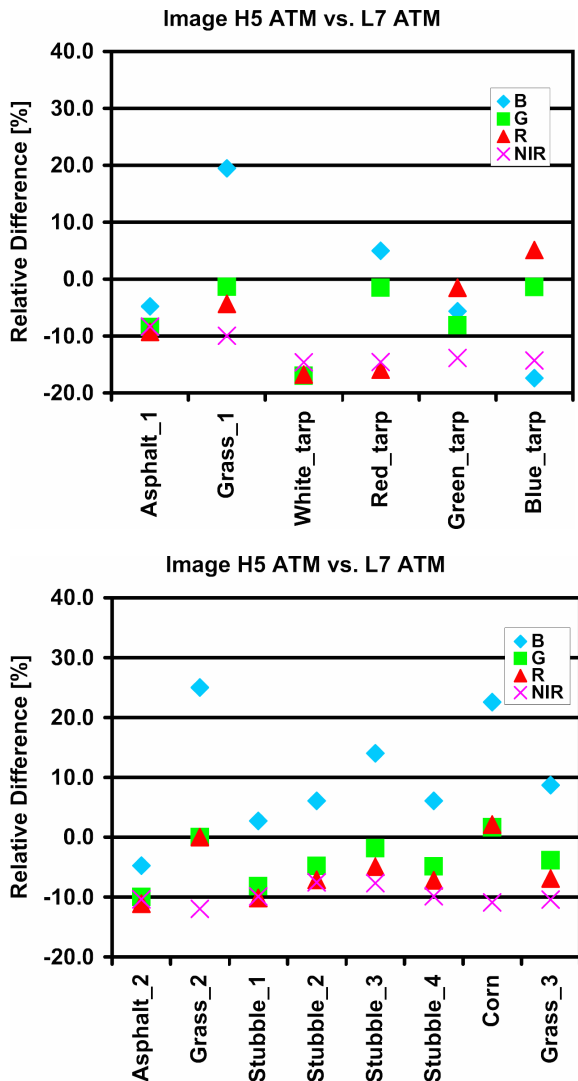
Contents
Author Index
Keyword Index

Figure 5. Relative differences of averaged image reflectances for different targets viewed from two flight lines from different altitudes, but with the same flight heading (N-S).

For a comparison of the atmospheric correction results of two different flight levels, again lines L7 and H5 were used (Figure 5). The relative difference of both was below 10% for Asphalt_1 and below 20% for Grass_1, and the colour tarps (Figure 5). For the additional vegetation targets in Figure 5 (e.g. Stubble_#), it can be seen that by averaging a large number of pixels (Table 2) the difference reduced to below 10% for R, G, and NIR. Only for the blue channel a larger discrepancy was found. This is attributed to atmospheric effects.

3.2 Validation of BRDF correction quality

To see the effect of the BRDF correction, the relative differences of the lines L4 (Backward) and L7 (Nadir) before and after the BRDF correction were evaluated using several large vegetation targets. As expected from the discussion in sec. 3.1, Figure 6 shows differences of up to 70% for the ATM corrected reflectances between the W−E and N−S flight lines L4 and L7.

After the BRDF correction, the differences for vegetation targets were generally below 10% for R, G, and B, and 20% for the NIR. Only the asphalt target showed a larger discrepancy.

This is due to the fact that the applied BRDF correction uses a correction function derived from an average statistics of the whole image. So some rare targets with a BRDF different from the average will not be corrected adequately.
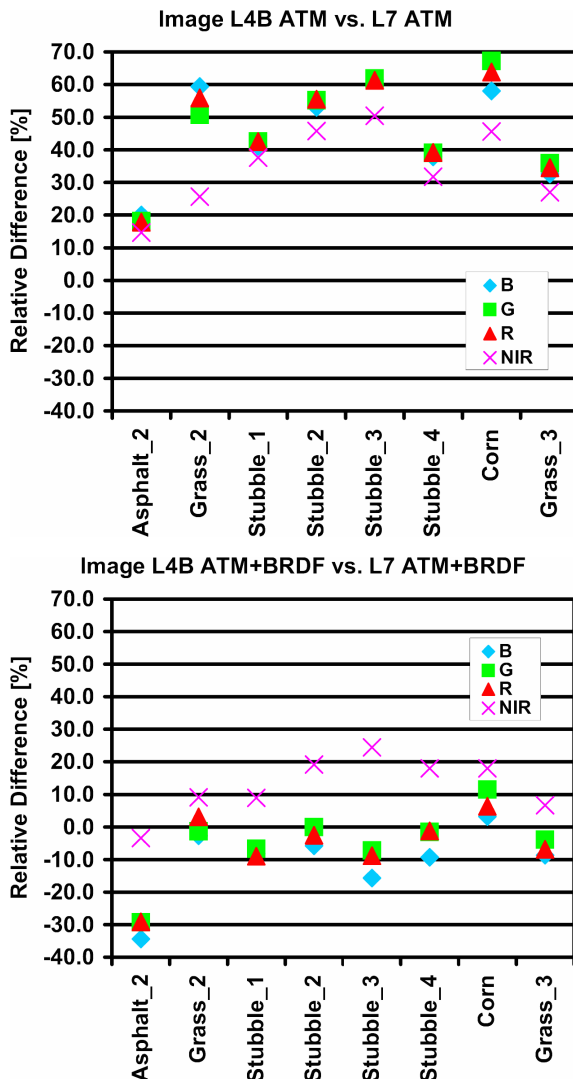

Figure 6. Relative differences of averaged image reflectances for different targets from a WE and a NS flight line of the same flight level before (top) and after (bottom) BRDF correction.

4. CONCLUSIONS

The project showed that ground reference targets used for validation (and also for in-flight calibration) have to be prepared carefully of non-specularly reflecting material and measured at the exact time of overflight. This is a tedious procedure and may be prohibitively expensive in most cases for routine remote sensing campaigns.

The ADS40/80 sensor together with the XPro "atmospheric" correction option enables the production of images with relative reflectance differences of less than 10% even for dark objects. The relative pixel-to-pixel accuracy is much higher, since the calibration and correction functions are smooth functions of the view angle.

To achieve this absolute accuracy, the following precautions have to be made. First, in the flight planning the flight line

In: Wagner W., Székely, B. (eds.): ISPRS TC VII Symposium – 100 Years ISPRS, Vienna, Austria, July 5–7, 2010, IAPRS, Vol. XXXVIII, Part 7B

Contents | Author Index | Keyword Index

headings have to be aligned to within ±25° with the sun azimuth of the expected flight time and day in order to avoid strong BRDF effects in the nadir line data. Second, a day with a cloudless sky is required in order to have a stable solar irradiation. A solar zenith angle of 30°–40° results in optimal illumination.

For standard photogrammetric projects those conditions cannot always be fulfilled, but also the radiometric requirements are lower. So, since the relative accuracy is much better and since the BRDF effects can be corrected to a visually pleasing result, the "atmospheric" or "atmospheric + BRDF" options are recommended as standard settings for data processing in ADS40-photogrammetry.

Integrating the use of measured ground spectra in the reflectance calibration process in XPro (inflight calibration) could enhance the absolute accuracy by calibration of the atmospheric correction parameters to the actual weather conditions. Also the integration of a class-specific BRDF-correction would improve the absolute accuracy in case the BRDF effects cannot be avoided.

ACKNOWLEDGEMENTS

REFERENCES

Alvarez, F., Catanzarite, T., Rodríguez-Pérez, J.R., and Nafria, D., 2010a. Radiometric calibration and evaluation of UltraCam X and Xp using portable reflectance targets and spectrometer data. Application to extract thematic data from the imagery gathered by the National Plan of Arial Orthophotography (PNOA). *Proc. EuroCOW2010*, 10.2.-12.2., Castelldefels, Spain.

Beisl, U., 2006. Absolute spectroradiometric calibration of the ADS40 Sensor. In: *Int. Arch. Photogramm. Remote Sens.*, Paris, France, Vol. XXXVI, part 1, 5 pp.

Beisl, U., Telaar, J., and Schönermark, M.v., 2008. Atmospheric correction, reflectance calibration and BRDF correction for ADS40 image data. In: *Int. Arch. Photogramm. Remote Sens.*, Beijing, China, Vol. XXXVII, part B7, pp. 7-12.

Bühler, Y. A., Hüni, A., Kellenberger, T. W., Itten, K. I., 2009. Towards an automated detection of avalanche deposits using their directional properties. *Proc. 6th EARSeL Workshop on Imaging Spectroscopy*, Tel Aviv.

Cramer, M., 2010a. The DGPF-test on digital airborne camera evaluation – overview and test design. In: *PFG 02-2010*, http://www.ifp.uni-stuttgart.de/dgpf/PDF/01-PFG02-2010-Ueberblick-FinalVersion-20100112.pdf (acc. 18 May 2010).

Cramer, M., 2010b. http://www.ifp.uni-stuttgart.de/eurosdr/ (accessed 18 May 2010).

Emmolo, D., Orlando, P., Villa, B., 2008. Evaluation of capabilities of fuzzy logic classification of different kind of data. In: *Int. Arch. Photogramm. Remote Sens.*, Beijing, China, Vol. XXXVII, part B7, pp 685-689.

Fraser, R. S., Ferrare, R. A., Kaufman, Y. J., Markham, B. L., and Mattoo, S., 1992. Algorithm for atmospheric corrections of aircraft and satellite imagery. *Int. J. Rem. Sens.*, 13(3), pp. 541-557.

González-Piqueras, J., Hernández, D., Felipe, B., Odi, M., Belmar, S., Villa, G., and Domenech, E., 2010. Radiometric aerial triangulation approach. A case study for the Z/I DMC. *Proc. EuroCOW2010*, 10.2.-12.2., Castelldefels, Spain.

Green, K., and Lopez, C., 2007. Using Object-Oriented Classification of ADS40 Data to Map the Benthic Habitats of the State of Texas. *Photogramm. Eng. Remote Sens.* 73(8), 861-865.

Honkavaara, E., Arbiol, R., Markelin, L., Martinez, L., Cramer, M., Bovet, S., Chandelier, L., Ilves, R., Klonus, S., Marshal, P., Schläpfer, D., Tabor, M., Thom, C., and Veje, N., 2009. Digital airborne photogrammetry — A new tool for quantitative remote sensing?—A state-of-the-Art review on radiometric aspects of digital photogrammetric images. *Remote Sensing* 1(3), pp. 577-605.

Kellenberger, T.W., and Nagy, P., 2008. Potential of the ADS40 aerial scanner for archaeological prospection in Rheinau, Switzerland. In: *Int. Arch. Photogramm. Remote Sens.*, Beijing, China, Vol. XXXVII, part B4, pp 1871-1877.

Markelin, L., Honkavaara, E., Peltoniemi, J., Ahokas, E., Kuittinen, R., Hyyppä, J., Suomalainen, J., and Kukko, A., 2008. Radiometric calibration and characterization of large-format digital photogrammetric sensors in a test field. *Photogramm. Eng. Remote Sens.* 74 (12), pp. 1487-1500.

Markelin, L., Honkavaara, E., Beisl, U., Korpela, I., 2010. Validation of the radiometric processing chain of the Leica ADS40 airborne photogrammetric sensor. *ISPRS TC VII Symposium: 100 Years ISPRS - Advancing Remote Sensing Science*, July 5-7, Vienna, Austria.

Molina, S., Villa, G., Serrano, C., Valdeperez, M., and Domenech, E., 2010. A polynomial approach for radiometric aerial triangulation. Proc. EuroCOW2010, 10.2.-12.2., Castelldefels, Spain.

Ryan, R. E., and Pagnutti, M., 2009. Enhanced absolute and relative radiometric calibration for digital aerial cameras. *Proc. Photogrammetric Week 2009*, Stuttgart, Germany.

Schönermark, M., 2010. Status report about the evaluation of the radiometric properties of digital photogrammetric airborne cameras, 2010. In: PFG 02-2010, http://www.ifp.uni-stuttgart.de/dgpf/PDF/05-PFG-02-2010-RadiometrieKalibrierung-FinalVersion-20100108.pdf (accessed 18 May 2010)

Waser, L.T., Eisenbeiss, H., Kuechler, M., and Baltsavias, E., 2008. Potential and limits of airborne remote sensing data for extraction of fractional canopy cover and forest stands and detection of tree species. In: *Int. Arch. Photogramm. Remote Sens.*, Beijing, China, Vol. XXXVII, part B8, pp 1405-1411.

Waser, L.T., Klonus, S., Ehlers, M., Küchler, M., and Jung, Andras, 2010. Potential of digital sensors for land cover and tree species classifications - a case study in the framework of the DGPF-project. In: *PFG 02-2010*, http://www.ifp.uni-stuttgart.de/dgpf/PDF/06-PFG-02-2010-RadiometrieKlassifizierung-FinalVersion-20100112.pdf (accessed 18 May 2010).